RSC Advances

ROYAL SOCIETY OF CHEMISTRY

www.rsc.org/advances

Synthesis of VO_2 nanoparticles by hydrothermal-assisted homogeneous precipitation approach for thermochromic applications

Wenjing Li,[a,b] Shidong Ji,[a] Yamei Li,[a,b] Aibin Huang,[a,b] Hongjie Luo[a,d] and Ping Jin[*a,c]

Abstract

Thermochromic VO_2 particles, which have potential application in "smart windows" for energy saving, have been successfully prepared by a convenient route combining homogeneous precipitation and hydrothermal processes. As a result, the particle size can be easily tuned from several tens to hundreds nanometers by controlling the initial vanadium source concentration. Lower concentration yielded large rod-like crystals, while high concentration obtained small near-spherical nanocrystals. The decrease of the size of VO_2 particles leads to an improvement in thermochromic properties, along with a wider hysteresis of the phase transition temperature. In addition, the W-doping can effectively tune the phase transition temperature (T_c) down to ambient with the efficiency about -21.3 ℃/at.%W in the doping range from 0 to 2.0 at.%W.

Introduction

Vanadium dioxide (VO_2) is a well-known material with complex polymorphs. In all these polymorphs, VO_2(M/R) has been extensively studied since it undergoes a reversible and abrupt semiconductor-metal transition (SMT) at around 340 K. Low-temperature monoclinicVO_2(M) is a semiconductor and infrared (IR) transparent while high-temperature rutileVO_2(R) is metallic and exhibits a high IR reflectance[1]. The drastic change in optical properties makes VO_2(M) a promising candidate for smart windows with thermochromic coating.

Traditionally, gas-phase-based preparation methods (e.g., sputtering, physical vapour deposition, chemical vapour deposition)[2] have been practiced by many researchers. However, these methods share common bottlenecks for practical applications, such as high cost and scale-up difficulties. As an alternative, high performance VO_2-based films have been fabricated by directly use high dispersed VO_2 nanoparticles in polymer matrix in recently years. This way shows numerous advantages, including convenience and versatility, low cost and potential for large-scale production[3]. Therefore, synthesis of high-quality VO_2 powders in the large availability is highly desired and urgently needed for preparing the VO_2-based films.

VO_2 powders have been prepared by many methods, such as pyrolysis of precursor powders[4], spray pyrolysis[5] and hydrothermal synthesis[6]. However, the pyrolysis process usually contains complicated route to prepare the vanadium precursor and the experiment condition is usually very harsh and energy-consuming[7]. And most of hydrothermal methods report the formation of the metastable phase (VO_2(B)) as the final products. In order to obtain the VO_2(M), it has to be annealed at high temperature[8]. The post annealing might lead to serious aggregation and make the method complex, which is unsuitable for the application. But to our knowledge, there have been several reports of one-step synthesis of VO_2(M) at low temperature recently, for example, the hydrothermal treatment of V_2O_4 in alcohol[9] and hydrothermal reaction of V_2O_5 with oxalic acid[10]. The products were mostly one-dimensional nanobelt, nanowire or microrod and the reaction time was more than two days. JungHo Son et al.[11] employed a combination of a hydrolyzed precipitate of VO^{2+} with hydrazine and NaOH to prepare VO_2(M) nanocrystals, but the products were mainly an mixture of VO_2(M) and VO_2(B) and the highest percent of VO_2(M) sized under 50 nm was less than 47% which might seriously affect the thermochromic properties in application for smart windows.

It could be found from the literatures that TiO_2[12], Al_2O_3[13], ZnO[14], CeO_2[15], SnO_2[16] and other metallic oxides can be prepared by homogeneous precipitation with urea. In the homogeneous precipitation process, the precipitates were proposed to arise from the decomposition of urea. Indeed, the urea used as homogeneous precipitation agent began to decompose and produce ammonia and carbon dioxide when the temperature was higher than 60 ℃. Due to the characteristics of urea, the pH of the solution could be increased very slowly and homogeneously throughout the whole solution which could avoid the phenomenon of high local concentration using direct precipitator. The gradual and uniform rise in pH can result in the nucleation and growth of uniformly nanosized particles. The products have many advantages, such as higher uniformity, narrow particle size distribution, higher surface area and good dispersion. So the homogeneous precipitation is a promising method for industrialization at present. However, no descriptions involved in preparation of VO_2 particles using homogeneous precipitation method have been published.

In this paper, a convenient one-step route for the preparation of thermochromic VO_2(M) particles has been developed by hydrothermal-assisted homogeneous precipitation approach. Differing from previous hydrothermal process, the proposed method is a convenient rout and utilizes inexpensive and low-toxic $VOSO_4$ as materials. The products have higher uniformity and controllable size. The particle size can be easily tuned form several tens to hundreds nanometers by controlling the initial vanadium source concentration, along with an improvement in optical properties.

Experimental

2.1 Synthesis of VO_2 (M)

All reagents were analytical grade and used without further purification. In a typical synthesis procedure, 0.815 g of $VOSO_4$ (Aladdin Reagent) and 0.6 g of $CO(NH_2)_2$ (AR, Aladdin Reagent) were mixed in 50 ml deionized water at room temperature with continuous magnetic stirring to form a blue transparent solution. An appropriate amount of $N_2H_4 \cdot H_2O$ (99%, Sigma Reagent) was diluted to 10 wt% with deionized water and then added to the solution. Under adequately stirring, the mixture was transferred into a 100 mL Teflon-lined autoclave. After the hydrothermal treatment at 260 ℃ for 24 h, the resulting black-colored precipitate was collected after being centrifuged and washed several times with deionised water and alcohol, and dried at 60 ℃ for 10 h. For the doped VO_2(M), different amount of tungstic acid (H_2WO_4, Wako Reagent) was added before sealing the Teflon-lined autoclave.

2.2 Characterization

The crystal structures of the samples were identified using X-ray powder diffraction (XRD, Model D/max 2550 V, Rigaku). The microstructures were observed by scanning electron microscope (SEM, JSM 6700F, JEOL) and transmission electron microscope (TEM, JEM-2010F, JEOL). The Raman spectrum was measured using a Raman microscope (Renishaw in Via). The phase transition behaviours of the products were measured by differential scanning calorimetry (DSC200F3, NETZSCH). The thermochromic properties of the films prepared by coating the powder onto a float glass substrate were conducted using a UV-Vis spectrophotometer (HITACHI U-3010) and the wavelength ranges from 350 nm to 2600 nm at 25 ℃ and 90 ℃.

Results and discussions

3.1 The mechanism of the reaction

No reaction occurred as long as the solution of $VOSO_4$ and urea remained at room temperature. The precipitates were proposed to arise from the decomposition of urea. Indeed, the urea used as homogeneous precipitation agent began to decompose and produce ammonia and carbon dioxide when the temperature was higher than 60 ℃. Due to the characteristics of urea, the pH of the solution may be increased very slowly and homogeneously throughout the whole solution. The gradual and uniform rise in pH can result in the nucleation and growth of uniformly nanosized particles. In the hydrothermal process, the reactions in the solution were as follows:

$$CO(NH_2)_2 + 3H_2O \rightarrow 2NH_4^+ + CO_2\,(g) + 2OH^-$$

$$VO^{2+} + 2OH^- \rightarrow VO(OH)_2\,(s) \rightarrow VO_2\,(s) + H_2O$$

During hydrothermal treatment, the urea worked as pH controller, which shifted the solution condition from original acidic to alkaline slowly. In order to react completely, the amount of urea should be excessive so we set the molar ratio of $VOSO_4$ to urea as 2 for all reactions.

In the system, it should be noted that the hydrazine hydrate which is a kind of strong reductant was the critical factor for the formation of VO_2(M) nanopowder. When only $VOSO_4$ and urea were used for precipitate formation without hydrazine hydrated, the products were mainly V_4O_9 with relatively little and poor crystallinity VO_2(M). The obvious strong intensity (200) peak (Fig.1a) of V_4O_9 at 10° indicated the good crystallinity. As it showed in Fig.1b, with increasing the amount of diluted hydrazine hydrate, the intensity of the V_4O_9 peaks was gradually decreased. On the contrary, there was an obvious increase in the intensity of VO_2(M) peaks. When the amount of diluted hydrazine hydrate was reached to 0.3 g, high purity of VO_2(M) with good crystallinity was prepared. We speculated that $VO(OH)_2$ was oxidized into V_4O_9 by the oxygen in the deionized water at high temperature without reducing agent. Further increasing the reducing agent produced lower valence vanadium oxide because of the stronger reducing ability of hydrazine. The addition amount of hydrazine should be controlled accurately. The hydrazine might played an important role as a coordinating ligand or reducing agent favoring the formation of VO_2(M) as the literature reported[11].

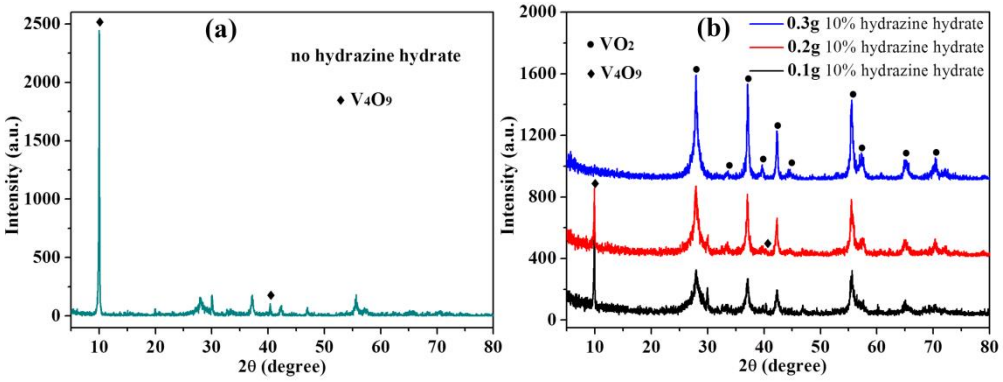

Fig. 1 XRD patterns of the products with (a) no hydrazine, (b) different amounts of diluted hydrazine hydrate.

3.2 Influence of the temperature

The reaction was carried out at different temperatures ranging from 180 to 260 °C to study the temperature effect. The results of the XRD patterns and SEM images were shown in Figure 2. A mixture of VO_2(B), VO_2(A), VO_2(M) and some other unknown impurities was formed at lower temperature (Fig.2a). With increasing the reaction temperature, a relatively high content of VO_2(M) was obtained. When the temperature reached to 260 °C, the product completely transformed to VO_2(M) (JCPDF Card NO. 43-1051, space group $P2_1/c$, a=5.752Å, b=4.538Å, c=5.383Å and β=122.64°). No peaks of any other phases or impurities were identified, which indicates the high purity and good crystallinity. The SEM images in Fig.2b-c all show two different morphologies: a platelike one and a granular one. At 180 °C, the products were almost plate like with rare granular particles compared with that at 220 °C. Further increasing the temperature to 260 °C could obtain a phase-pure VO_2(M) with single uniform granular structure as shown in Fig.2d. The morphology of the phase-pure VO_2(M) is shown in Fig.3 as a relatively enlarged TEM image, which clearly proved its uniform granular structure with an average size of 20-70nm.The Raman spectra (Fig.4) also confirmed the composition and phase of the product obtained at 260 °C. The Raman modes located at 192, 223, 263, 309, 340, 387, 499 and 613 cm^{-1} are assigned to monoclinic VO_2 (M) in accordance with the previous report[17].

It could be supposed that when the temperature was higher than 60 ℃, the urea began to decompose and

produce ammonia which reacted with VO^{2+} to form the granular $VO(OH)_2$ precipitation. The $VO(OH)_2$ particles were aggregated and grew into platelike product at lower temperature, however, it could keep its original morphologies and crystallized into VO_2(M) when maintained at a higher temperature.

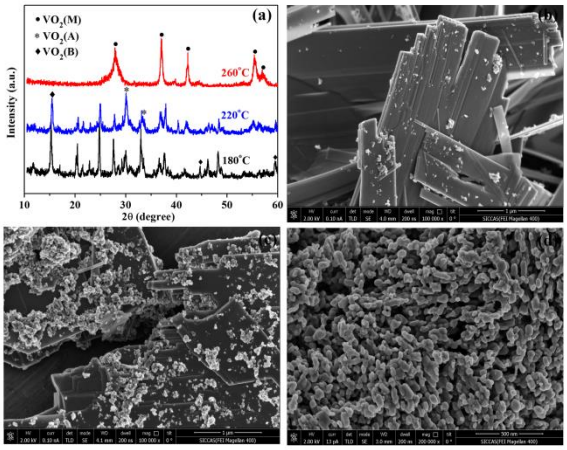

Fig. 2 (a) XRD patterns of the products obtained at different hydrothermal reaction temperatures. (b-d) SEM images of the products obtained at different hydrothermal reaction temperatures: (b) 180 ^{o}C, (c) 220 ^{o}C, (d) 260 ^{o}C.

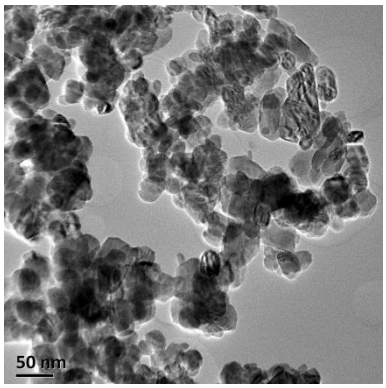

Fig. 3 TEM image of the product obtained at 260 ^{o}C.

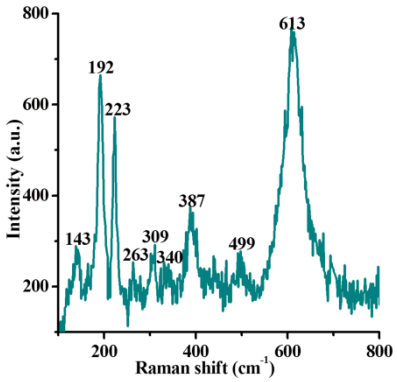

Fig. 4 Raman spectra of the prepared powders at 260 ^{o}C

3.3 Influence of the concentration of vanadium precursor.

Under careful control of the amount of hydrazine hydrate and hydrothermal reaction temperature, pure single phase VO_2(M) could be obtained. The lateral dimensions and morphology of the products depended on the initial vanadium concentration. Fig.5a shows the typical XRD patterns of VO_2 particles produced with various vanadium concentrations. All peaks can be indexed to VO_2(M). The Sample C (0.05 mol L^{-1}) exhibited the highest (011) peak intensity and the minimum of full width at half maximum (FWHM), indicating higher crystallinity and bigger grain size compared with other samples. The final particle size and morphology of VO_2(M) with various vanadium concentrations were depicted in Fig.5b-d. High concentration of vanadium yielded granular nanocrystals (Sample

A in Fig.5b) around 20~50 nm, while lower concentration of vanadium yielded short rod-like crystals (Sample B in Fig.5c). When the concentration tuned down to much lower, the rod-like crystals grew longer (Sample C in Fig.5d) with ~100 nm in diameter and ~500 nm in length.

The phenomenon could be interpreted as a result of the different levels of supersaturation which increased along with the increasing vanadium concentration at the same temperature. A lower concentration of vanadium would favor the formation of fewer nucleus, thus making the crystals grow longer to form the big crystals. In contrast, with increasing the concentration, the nucleation rate and growth rate all became larger while the nucleation rate grew faster, which caused greater chance to form VO_2(M) seeds and obtained smaller particles at the end. The particle size can be easily tuned from several tens to hundreds nanometers by controlling the initial vanadium source concentration.

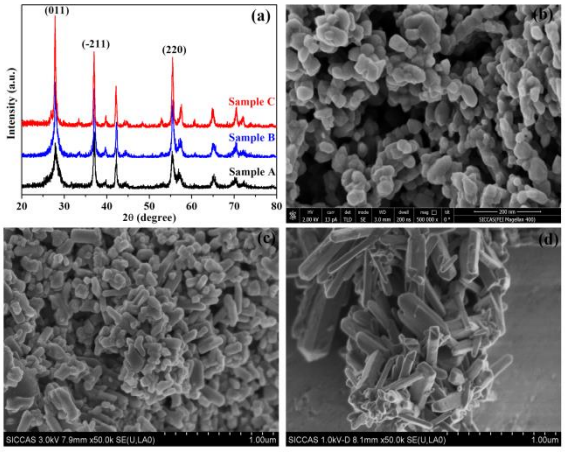

Fig. 5 (a) XRD patterns of the products obtained at different concentrations of $VOSO_4$. (b-d) SEM images of the products obtained at different concentrations of vanadium: (b) Sample A 0.5 mol L^{-1}, (c) Sample B 0.1 mol L^{-1}, (d) Sample C 0.05 mol L^{-1}.

The reversible phase transition temperatures (T_c) of the Samples were measured by differential scanning calorimetry (DSC) and the DSC curves are shown in Fig.6. The T_c of Sample A, B and C were 65.6, 64.8 and 65.0 ^oC (Table 1), respectively, which were all slightly lower than 340 K in single crystals reported firstly by Morin[18]. The increased dimension of VO_2 particles from Sample A to Sample C led to a slightly decreased transition temperature (from 65.6 ^oC to 65.0 ^oC) and an obvious narrowed hysteresis (from 16.2 ^oC to 11.5 ^oC) as showed in Table 1. This phenomenon was similar to the literatures reported by Zhenda Lu et al.[19] and R. Lopez et al.[20]. The observed hysteresis broadening of VO_2 particles may originate from the greater number of [VO_6] octahedra located at the smaller nanostructure surfaces where some distortions in bonding may be possible as a result of surface reconstruction or lattice expansion[19].

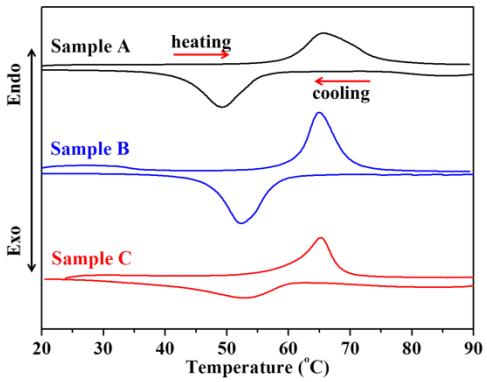

Fig. 6 DSC curves of the Samples obtained in different concentration of $VOSO_4$ (Sample A is 0.5 mol L^{-1}, Sample B is 0.1 mol L^{-1}, Sample C is 0.05 mol L^{-1}).

The films were prepared by coating the powders onto a float glass substrate and measured at 25 ℃ and 90 ℃ from 350 nm to 2600 nm. The infrared (IR) modulations at 1000, 1500, 2000 and 2500 nm were 14.5, 29.3, 36.1and 38.1% respectively for Sample A; 18.4, 34.9, 40.8 and 40.9% for Sample B and 11.4, 22.2, 26.5 and 28.4% for Sample C (Fig.7). The Sample B had relatively higher IR modulations but weak Solar modulation ability (ΔT_{sol}) compared to Sample A (from 7.6% to 7.4% in Table 1). The cause was that the change in the visible transmittance (T_{vis}) for Sample B (from 11.7% to 16.6%) was bigger than Sample A (from 20.6% to 21.4%). In general, Sample

A with the smallest size had the optimal optical properties. Therefore, it seems that further reducing the particle size of theVO_2may have advantages in improving the optical properties of the films.

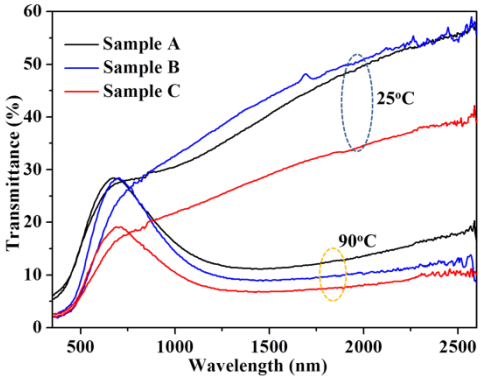

Fig. 7 The transmittance spectra of the films for different Samples (Sample A is 0.5 mol L^{-1}, Sample B is 0.1 mol L^{-1}, Sample C is 0.05 mol L^{-1}).

For all the films, the Visible transmittance (T_{vis}, 400-700nm), Solar transmittance (T_{sol}, 350-2600nm) and Solar modulation ability (ΔT_{sol}) were obtained based on the measured spectra using the following equation:

$$T\rho = \int \psi_\rho(\lambda) T(\lambda) d\lambda / \int \psi_\rho(\lambda) d\lambda$$

Where $T(\lambda)$ means the transmittance at wavelength λ; ρ denotes *vis*or *sol* for calculations; ψ_{vis} is the standard efficiency function for photopic vision; and ψ_{sol} is the solar irradiance spectrum for an air mass of 1.5 (corresponding to the sun standing 37° above the horizon)[21]. In the Table1, $\Delta T_{sol} = T_{sol,l} - T_{sol,h}$, l and h represent 25°C and 90 °C, respectively, in the measure.

Table 1. Phase transition temperatures, hysteresis and optical properties for Sample A, B and C.

Sample	T_c-DSC (°C)		ΔT_c (°C)	T_{vis} (%)		T_{sol} (%)		ΔT_{sol} (%)
	heating	cooling		25 ℃	90 ℃	25 ℃	90 ℃	
A	65.6	49.4	16.2	20.6	21.4	26.2	18.6	7.6
B	64.8	52.5	12.3	11.7	16.6	23.4	16.0	7.4
C	65.0	53.5	11.5	9.4	11.7	16.3	11.3	5.0

3.4 Influence of the W-doping

Fig.8a showed the XRD patterns of the products with various amount of W doping and the typical diffraction peaks could be perfectly indexed to the VO_2(M). No tungstic acid and other vanadium oxides were observed, which revealed that the products were well-crystallized with high purity. Compared to the undoped sample, W doping had little influence on the crystal structure of the VO_2(M) but had no obvious effect on the morphology of the particles (Fig. S1, ESI†). When the amount of W-doping increased, all the peaks of the doped samples were slightly shifted towards a lower 2θ value. The magnification of the (011) peaks (shown by the blue oval in Fig.8a) were displayed in Fig.8b. Table 2 showed the shift of the main peak position of the W-doping VO_2(M) XRD patterns. The phenomenon could be due to the fact that the radius of W atoms was larger than that of V atoms. When the amount of W-doping increased, more V ions in the monoclinic lattice would be substituted by W ions. Therefore the adjacent interplanar distance would expand with resulting that all of the peaks shifted towards a lower angle according to the Scherrer equation ($2d\sin\theta = \lambda$). This could further confirm that W had been successfully incorporated into the crystal lattice of VO_2(M). The precise amounts of W doping in the VO_2 detected by coupled plasma measurement (ICP) were also listed in Table 2.

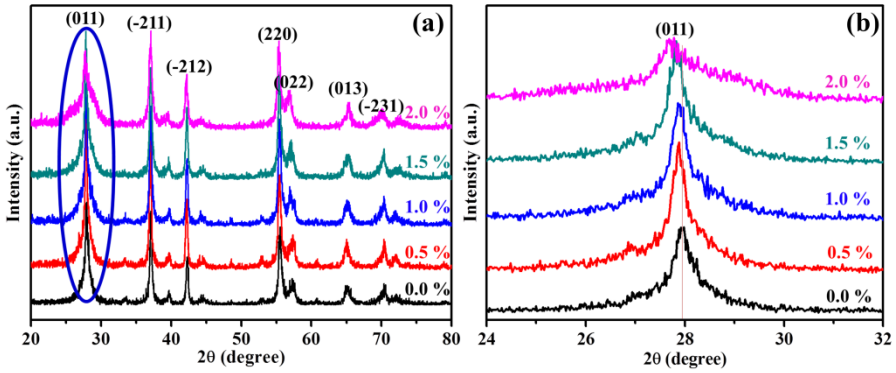

Fig. 8 (a) XRD patterns, (b) a magnified pattern of the (011) peak of the obtained VO_2 powders with different W-doping fractions.

Table 2 The position of the main peak in the VO_2(M) and the precise amount of W-doping detected by ICP.

Sample	W-doping content (at%)	ICP (at%)	2θ (°)
W1	0	0	27.92
W2	0.5	0.44	27.88
W3	1	0.93	27.86
W4	1.5	1.35	27.78
W5	2	1.79	27.72

The oxidation states of vanadium and tungsten of the W-doped VO_2 sample were performed by X-ray photoelectron spectroscopy (XPS) as shown in Fig. 9, which indicated that the sample only consisted of four elements, including carbon, vanadium, oxygen and tungsten. The peak of carbon could be attributed to the surface contamination. From Fig. 9b, the peak of O_{1s} appeared at its standard value (530.0 eV) and the other peaks at 524.1 eV and 516.5 eV were attributed to $V_{2p1/2}$ and $V_{2p3/2}$, respectively. The value of $V_{2p3/2}$ was slightly higher than that of pure VO_2[22], but was in agreement with the value 516.3 eV studied by Li[23] for $V_{0.99}W_{0.001}O_2$, which suggested that the binding energy of $V_{2p3/2}$ increased slightly after W-doping and the vanadium of the doped sample was exhibited +4 oxidation states. Fig. 9c showed that the W_{4f} peaks of the sample with binding energies of $W_{4f5/2}$ and $W_{4f7/2}$ centered at 37.7 and 35.7 eV, respectively. According to the standard binding energy, it was shown that there was a little tungsten in the sample, and the oxidation state of tungsten ion in these nanopowders was W^{6+} instead of other valence form[24].

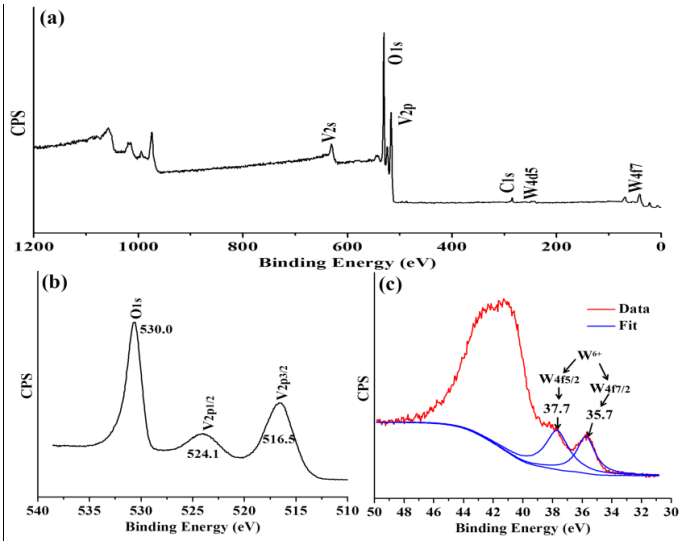

Fig. 9 XPS spectra for W-doped VO_2: (a) survey spectrum, (b) core-level spectrum for V_{2p} and O_{1s}, and (c) core-level spectrum for W_{4f}.

The phase transition properties of the VO_2 with different doping content were investigated by DSC. The peak

located at 64.8 °C was corresponded to the pure VO_2. After doping W into the VO_2 crystal lattice, the T_c was reduced to 52.5, 43.3, 33.5 and 21.9 ℃ corresponding to the doping fraction of 0.5, 1.0, 1.5 and 2.0 at.% (Fig.10a), respectively. The relationship between the T_c and doping amount was an oblique line (Fig.10b) and the slope was 21.3 ℃/at.%W which was consistent with the previous literatures[7, 25]. The results indicated that the W element could be effectively doped into the VO_2 lattice and easily tune down the T_c in this system. According to the reported model of Tang et al.[26], W^{6+} ion was diffused into the crystal lattice of VO_2(M) and substituted the V^{4+} ion. With the increasing fraction of W^{6+} in the lattice, the loss of V^{4+}-V^{4+} pairs which are essential for the crystal structure of the semiconducting VO_2 phase[1] became much more obvious. It resulted in destabilizing the semiconducting VO_2 phase and consequently lowered the semiconductor-metal phase transition temperature. At the same time, the driving force for the semiconductor-metal transition is the increase in electronic energy; the transition occurs only when increasing of electronic energy more than counteracts the strain energy induced by lattice distortions[27]. Doping with high valence W^{6+} ion could increase the concentration of free electrons and promote the transition at lower temperature. Slightly doping with W element did not decrease the optical properties while highly doped samples showed lower thermochromic effect in the infrared area. The IR modulation at 2000 nm for undoped sample was 41% while the 1.0 at.% and 1.5 at.% W-doping samples were decreased to 27% and 18%, respectively (Fig. S2, ESI†).

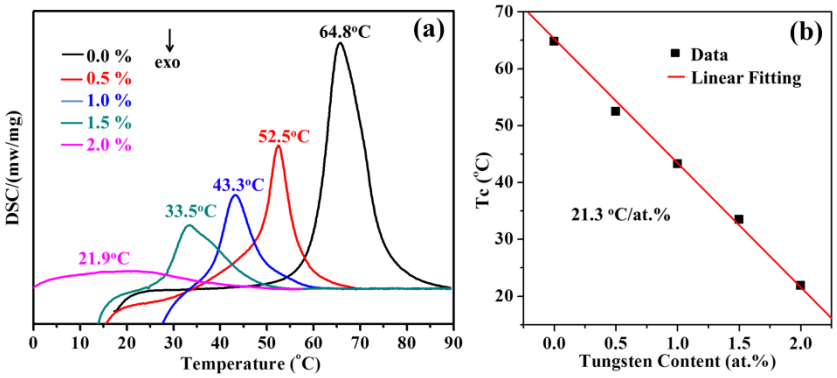

Fig. 10 (a) DSC curves, and (b) the T_c data with linear fitting of the obtained VO_2 powders with different W-doping fractions.

Conclusion

We have developed a novel one-step route combining homogeneous precipitation and hydrothermal processes for the fabrication of size-controlled VO_2(M) particles. The proposed method is remarkably convenient and affordable, which utilizes inexpensive and low-toxic materials. The as-prepared VO_2 products exhibit a size dependent effect in the optical properties and the phase transition. The decreased dimension of VO_2 particles led to an improvement in the optical properties, along with a slightly increased transition temperature and wider hysteresis, In the system, W element could be effectively doped into VO_2 lattice and the T_c reduction efficiency was about -21.3 ℃/at.%W in the doping range from 0 to 2.0 at.%W.

This study was financially supported by the National Key Basic Research Program (NKBRP, 2009CB939904), and the high-tech project of MOST (2012AA030605, 2012BAA10B03), and the National Natural Science Foundation of China (NSFC, No: 51032008, 51272273, 51102270, 51272271, 51172265, 51372264), and Science and Technology Committee of Shanghai (No: 13PJ1409000).

Notes and references

[a] *State Key Laboratory of High Performance Ceramics and Superfine Microstructure, Shanghai institute of Ceramics, Chinese Academy of Sciences, Dingxi 1295, Changning, Shanghai, 200050, China, Tel/Fax:+86-21-6990-6208 Email: p-jin@mail.sic.ac.cn.*
[b] *Graduate School of Chinese Academy of Sciences, Beijing 100049,China*
[c] *Materials Research Institute for Sustainable Development, National Institute of Advanced Industrial Science and Technology(AIST), 2266-98 Shimoshidami, Moriyama-ku, Nagoya 463-8560, Japan*
[d] *School of Materials Science and Engineering, Shanghai University, Shangda Rd.99, Baoshan District, Shanghai 200444, China*
† Electronic Supplementary Information (ESI) available: [details of any supplementary information available should be included here]. See DOI: 10.1039/b000000x/
‡ Footnotes should appear here. These might include comments relevant to but not central to the matter under discussion, limited experimental and spectral data, and crystallographic data.
1. A. Zylbersztejn and N. F. Mott, *Phys. Rev. B*, 1975, **11**, 4383-4395.

2. J. D. Zhou, Y. F. Gao, X. L. Liu, Z. Chen, L. Dai, C. X. Cao, H. J. Luo, M. Kanahira, C. Sun and L. M. Yan, *Phys. Chem. Chem. Phys*., 2013, **15**, 7505-7511.
3. J. Zou, Y. G. Peng and H. Lin, *J. Mater. Chem. A*, 2013, **1**, 4250-4254.
4. J. Q. Shi, S. X. Zhou and B. You, *Sol. Energy Mater. Sol. Cells*, 2007, **91**, 1856-1862.
5. S. A. Lawton and E. A. Theby, *J. Am. Ceram. Soc.*, 1995, **78**, 104-108.
6. S. D. Ji, Y. G. Zhao, F. Zhang and P. Jin, *J. Cryst. Growth*, 2010, **312**, 282-286.
7. S. D. Ji, F. Zhang and P. Jin, *Sol. Energy Mater. Sol. Cells*, 2011, **95**, 3520-3526.
8. K. F. Zhang, X. Liu, Z. X. Su and H. L. Li, *Mater. Lett.*, 2007, **61**, 2644-2647.
9. Whittaker L., Jaye C., Fu Z., Fischer D. A. and Banerjee S., *J. Am. Ceram. Soc.*, 2009,**131**, 8884-8894.
10. C. X. Cao, Y. F. Gao and H. J. Luo, *J. Phys. Chem. C*., 2008, **112**, 18810-18814.
11. J. H. Son, J. Wei, D. Cobden, G. Z. Cao and Y. N. Xia, *Chem. Mater.* , 2010, **22**, 3043-3050.
12. S. J. Kim, S. D. Park and Y. H. Jeong, *J. Am. Ceram. Soc.*, 1999, **82**, 927-932.
13. P. Bai, F. B. Su, P. P. Wu, L. K. Wang, F. Y. Lee, L. Lee, Z. F. Yan and X. S. Zhao, *Langmuir*, 2007, **23**, 4599-4605.
14. L. X. Zhang, J. H. Zhao, H. Q. Lu, L. M. Gong, L. Li, J. F. Zheng, H. Li and Z. P. Zhu, *Sensor. Actuat. B: Chem.*, 2011, **160**, 364-370.
15. H. Y. Chen and H. Y. Chang, *Colloid. Surface. A: Physicochem. Eng. Aspects*, 2004, **242**, 61-69.
16. K. C. Song and Y. Kang, *Mater. Lett.*, 1999, **42**, 283-289.
17. T. D. Manning, I. P. Parkin, M. E. Pemble, D. Sheel and D. Vernardou, *Chem. Mater.*, 2004, **16**, 744-749.
18. F. J. Morin, Phys. *Rev. Lett.*, 1959, **3**, 34-36.
19. Z. D. Lu, C. G. Li and Y. D. Yin, *J. Mater. Chem.*, 2011, **21**, 14776-14782.
20. R. Lopez, T. E. Haynes and L. A. Boatner, *Phys. Rev. B*, 2002, **65**, 2241131-1141135.
21. Y. J. Zhou, A. B. Huang, Y. M. Li, S. D. Ji, Y. F. Gao and P. Jin, *Nanoscale*, 2013, **5**, 9208-9213.
22. G. Silversmit, D. Depla, H. Poelman, G. B. Marin and R. D. Gryse, *J. Electron Spectrosc.*, 2004, **135**, 167-175.
23. F. Li, X. H. Wang, C. L. Shao, R. X. Tan and Y. C. Liu, *Mater. Lett*., 2007, **61**, 1328-1332.
24. Z. F. Peng, W. Jiang and H. Liu, *J. Phys. Chem. C*, 2007, **111**, 1119-1122.
25. A. B. Huang, Y. J. Zhou, Y. M. Li, S. D. Ji, H. J. Luo and P. Jin, *J. Mater. Chem. A*, 2013, **1**, 12545
26. C. Tang, P. Georgopoulos, M. E. Fine, J. B. Cohen, M. Nygren, G. S. Knapp and A. Aldred, *Phys. Rev. B*, 1985, **31**, 1000-1011.
27. L. Whittaker, C. J. Patridge and S. Banerjee, *J. Phys. Chem. Lett.*, 2011, **2**, 745-758.

Senior Editor
Royal Society of Chemistry
Dear Dr S. Richards:
Sorry for disturbing you. Thank you for your kind considerations on our manuscript titled "Synthesis of VO_2 nanoparticles by hydrothermal-assisted homogeneous precipitation approach for thermochromic applications" (Manuscript ID: RA-ART-12-2013-047666). We have tried our best to finish the revisions in accordance with the editor and the reviewers' comments as soon as possible. However, due to the Spring Festival holiday, we spent a long time to wait for the result of the test of XPS analysis which is a key point to reply the reviewers and it will still need one week. We will provide our revised manuscript before 17-Feb-2014, please let us know if it is ok.
Best Regards
Yours, sincerely

Thank you very much for your letter and the comments about our manuscript (ID RA-ART-12-2013-047666) had been received. And we also thank the reviewers for their instructive comments that are undoubtedly beneficial to the manuscript. It is so long time to wait for the test of XPS analysis during the Spring Festival holiday. Thus the reply might be delayed and we are very sorry for it. We will provide our revised manuscript as soon as possible and please give us some time.